

## Resistance Spot Welding of Steels: Modeling and Simulation

M. Valaee <sup>1</sup>, M. Sheikhi \*<sup>2</sup>, Y. Mazaheri <sup>3</sup>, G.R. Usefifar <sup>4</sup>

<sup>1,2,3</sup> Department of Materials Engineering, Bu-Ali Sina University, Hamedan, Iran

<sup>4</sup> SAIPA Corporation, Tehran, Iran

### Abstract

Resistance spot welding (RSW) includes many variables that can influence the weld properties. The purpose of this study is to develop an analytical model for prediction of thermal history and weld microstructure in RSW and to find the most important process parameters that influence the weld microstructure. A one dimensional model is proposed for prediction about thermal history during cooling step of RSW process. The reliability of analytical model is evaluated by experiments and numerical simulations. The calculations reveal that the current analytical model is reliable particularly at the temperatures lower than  $T_m/2$ . Sheet surface temperature at electrode-sheet interface and sheet thickness are recognized as the most important factors affecting the cooling rate at  $T < T_m/2$ . Austenite decomposition is one of the most important transformations in steels that occurs in this temperature interval. Finally an easy to use map also is developed based upon the present analytical model for prediction of weld microstructure.

*Keywords:* Resistance welding; Simulation; Modeling; Weld microstructure; Cooling rate.

### 1. Introduction

Spot resistance welding is one of the most prevalent welding processes in sheet metal joining and automotive industry. The weld properties are affected by many variables, which include resistance spot welding (RSW) process and many investigations have been done to understand these relationships <sup>1-4</sup>. It is demonstrated that the weld strength, impact resistance and formability of produced weld by RSW process are mainly depended on the nugget dimensions (diameter and penetration) <sup>1,2</sup>. The mechanical properties of the produced joint also are deeply depended on the weld integrity and its microstructure <sup>1,2,5</sup>.

It is important to find that how operating conditions influence the above factors. Numerical simulation is

the best alternative method to understand the RSW mechanism which helps determine suitable welding parameters required to reach an appropriate weld. Eisazadeh et al. <sup>6</sup> showed that as welding current increased, the growth rate of nugget decreased until expulsion happened. Also it is found that welding current is a dominant factor to determine the nugget size compared with time. Nodeh et al. concluded that the maximum residual stress can be found at the center of the nugget <sup>7</sup>. Weld expulsion occurrence has also been analyzed by finite element simulation and it is founded that the initial gap between the sheets is a critical factor <sup>8</sup>.

In addition, the numerical modeling approved that in comparison to welding time, welding current plays a more important role in the nugget formation <sup>9</sup>. In contrast to the considerable investigations on simulation of RSW <sup>6-13</sup>, small part of studies focused on development of analytical models to predict the nugget size or temperature history during RSW <sup>4,14</sup>.

The purpose of this study is to put forward a thermal model during cooling step in order to get better understanding of RSW process and to predict the cooling rate and in turn the resultant weld microstructure.

\* Corresponding Author

Tell: +98 81 38257400

Email: sheikhi.mohsen@basu.ac.ir

Address: Department of Materials Engineering

Bu-Ali Sina University, Hamedan, Iran

1. M.Sc. Student

2. Assistant Professor

3. Assistant Professor

4. M.Sc.

To evaluate the analytical model, a quarter of symmetric models solution domain was analyzed using finite element method. In order to assess the calculations, the effect of current on the weld properties made on two interstitial free steels were experimentally investigated.

**2. Experiments and Methods**  
**2.1. Materials and procedures**

In this study two low carbon steel sheets of 0.7 mm thickness were used for welding. The chemical compositions and mechanical properties of used materials are given in Table 1.

The spot welding process was carried out with a single phase, 55 kVA and 50 Hz AC machine. A pair of water cooled Cu-Cr alloy cone flat type electrodes of 6.0 mm face diameter was employed for welding. Welding operating conditions are given in Table 2.

It should be mentioned that except welding current all other welding parameters was kept constant during the operation. It should also be mentioned that in this research, the root mean square value of welding current is reported as welding current.

To examine the weld microstructures by optical microscopy, the weld samples were sectioned across the nugget. Then they were grinded, polished and etched by 2% Nital reagent. In order to determine the hardness profile of the welding zone, Vickers micro-hardness test was utilized at 100 gr loading condition. For each sample, the hardness profiles were determined on weld cross section and along two different paths: (1) along nugget diameter (r axis in Fig. 1) and (2) along nugget depth (along z axis in Fig. 1). Also the weld zone dimensions and macrostructure of the welds were characterized using a stereo microscope.

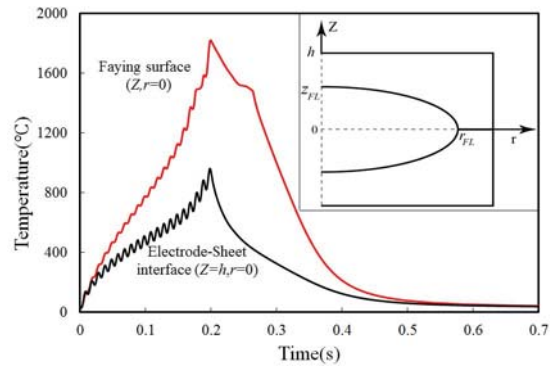


Fig. 1. Thermal histories at the faying surface and sheet-electrode interface for weld created with 12kA welding current.

**2.2. Modeling and simulation**

Regarding the previous investigations<sup>4,14</sup>, it is reasonable to assume that the bulk of heat transfer takes place by conduction through water cooled electrodes and along sheet thicknesses (z axis in Fig. 1). Accordingly, one dimensional heat transfer governing equation is considered to develop an analytical model during cooling step:

$$\frac{\partial T}{\partial t} = \alpha \frac{\partial^2 T}{\partial z^2} \tag{Eq. (1)}$$

In this equation t is time after cutting off the current,  $\alpha$  is heat diffusivity and it is equal  $k/\rho c_p$  where k is thermal conductivity,  $\rho$  is density and  $c_p$  is specific heat. About boundary condition, it is assumed that the electrode- sheet contacts have the ideal condition and thermal resistance can be ignored in this contact.

Table 1. Mechanical properties and chemical composition (in wt. %) of two steel sheets used in this study.

Hardness (Hv)	Ultimate tensile strength (MPa)	Yield strength (MPa)	Chemical composition				
			C	Mn	Si	Ni	Cr
80	265	145	0.02	0.15	0.01	0.03	0.04

Table 2. Welding operating parameters used in the experiments.

Squeeze time (cycle)	Welding time (cycle)	Holding time (cycle)	Welding current (kA)	Electrode force (kN)
10	10	10	8, 10, 12	50

Therefore, it is assumed that the temperatures of the outer sheet surface ( $T_s$ ) and electrode surface at the above interface will be remained equal during cooling step. In other words:

$$T(z = h, t) = T_s \tag{Eq. (2)}$$

The analytical solution of this equation can be done using separation variable method. In this method, temperature function is only expressed as a function product of position ( $F(z)$ ) and a function of time only. Accordingly the initial condition can be stated as follows:

$$T(z, t = 0) = F(z) \tag{Eq. (3)}$$

Where here  $F(z)$  is the temperature distribution along  $z$  direction at the moment of current termination. Regarding the obtained results from numerical model for temperature profile along sheet thickness at  $t=0$ , which are also in line with previous investigations<sup>6-10</sup>, it is approximately good assumption to estimate the temperature profile by a sinusoid. Therefore, the following equation is proposed for positional function:

$$F(z) = (T_{max} - T_s) \cdot \cos\left(\frac{\pi}{2h} z\right) + T_s \tag{Eq. (4)}$$

Therefore the solution of Eq. (1) based upon separation variable method leads to the following equation:

$$T(z, t) = (T_{max} - T_s) \cdot \cos\left(\frac{\pi}{2h} z\right) \exp\left(-\frac{\alpha\pi^2}{4h^2} t\right) + T_s \tag{Eq. (5)}$$

It should be mentioned that regarding the large dependency of specific heat, thermal conductivity and density to temperature and in order to reduce the error in the calculations, the average value of these parameters between solidus and room temperature is considered for computations of thermal diffusivity which leads to  $\alpha \cong 2.7 \times 10^{-6}$ . The released latent heat during solidification is neglected that it can cause some indecision over solidification interval.

The temperature of the electrode-sheet interface ( $T_s$ ) changes during welding. In order to compute the electrode-sheet interface temperature, with the assumption of the linear temperature gradient in the electrode, the boundary condition can be summarized at  $z=h$  as follows:

$$k_E \frac{T_s - T_w}{Z_E} = k_s \frac{\partial T}{\partial z} \tag{Eq. (6)}$$

, where  $k_E$  is electrode thermal conductivity and  $Z_E$  is electrode face thickness. So  $T_s$  can be obtained by combining Eqs. (5) and (3). Hence:

$$T_s = T_{max} - \frac{T_{max}}{1 + \frac{\pi k_s Z_E}{2h k_E} \exp\left(-\frac{\alpha\pi^2}{4h^2} t\right)} + T_w \tag{Eq. (7)}$$

In order to evaluate the proposed analytical model, the welding process was simulated by finite element package ABAQUS. Due to the symmetry of the process only a quarter of welding zone was modeled using 3D model which was appropriate for the initial and boundary condition applied on it. The initial condition is the initial temperature of the sheets and electrodes which reasonably room temperature was considered for them. Welding current was applied by surface current load with uniform distribution at the top surface of the upper electrode. Regarding the excessive temperature changes experienced by welding zone and large temperature dependency of material and contact properties such as electrical and thermal conductivity, temperature dependent properties were applied to the numerical model as given in the reference<sup>15</sup>. In the simulation, heat loss due to the convection on the outer surfaces of the sheets and electrodes are also taken into account. It is assumed that the temperature of water cooled electrode surfaces during the welding process does not change and it is kept constant and equal to water temperature. Simulation results were validated by the comparison between experimental nugget dimensions and predicted ones using the numerical method. It should be mentioned that weld pool convection was ignored in the calculations.

### 3. Results

#### 3.1. Hardness and microstructure

Fig. 2 shows a typical micro-hardness profile of welded sample with 8 kA. These measurements were carried out along two different paths: the nugget diameter and nugget penetration. The hardness distribution of the other samples follows the similar trend. The average values of measured hardnesses at the nugget zone (NZ) and lateral heat affected zone (HAZ) for all welded samples summarized in Fig. 2. Despite the expectations, it is seen that the average hardness of both nugget and heat affected zones increase as the welding current increases from 8 kA to 10 and 12 kA. Fig. 3 illustrates the details of the microstructure of weld made with 8 kA. As can be seen, the nugget microstructure contains martensite phase.

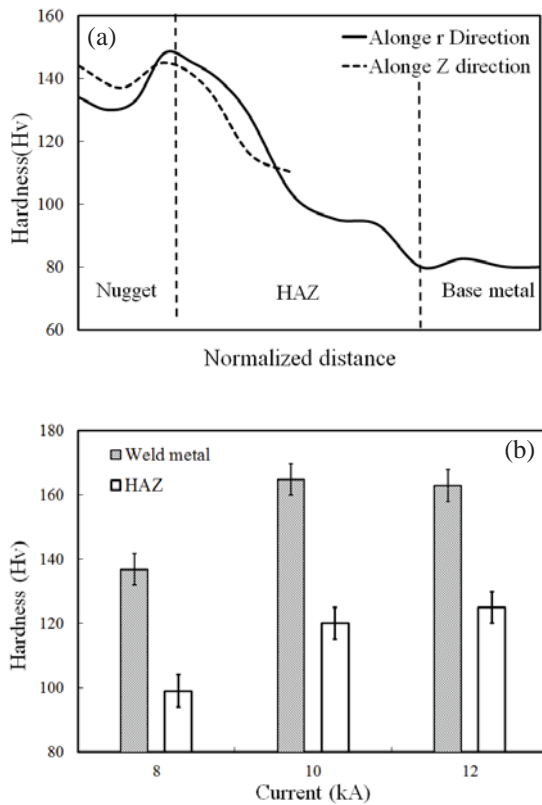


Fig. 2. The variation of hardness in the welding zones. (a) hardness profile along the nugget diameter ( $r$  direction) and the nugget penetration ( $z$  direction) for welded sample with 8 kA, (b) the average hardness of the nugget and HAZ correspond to different welding conditions.

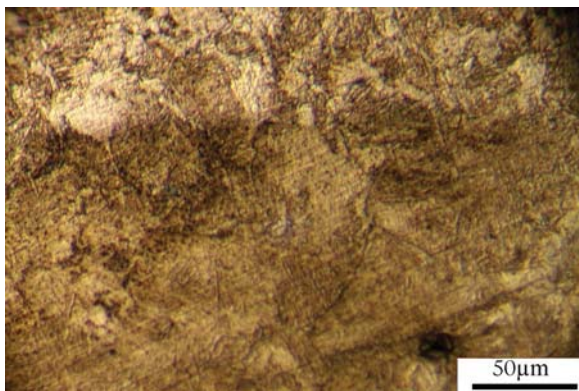


Fig. 3. The microstructure of the nugget formed with 10 kA.

### 3.2. Simulation results

The process parameters were applied to the numerical model to calculate the nugget dimensions and thermal histories of welding zone under different welding conditions.

The validation of numerical results was undertaken by comparison between the available nugget dimensions with predicted ones. In the simulations, NZ is considered as the region that experiences peak temperatures above 1520 °C. These comparisons reveal that the numerical model can estimate the nugget dimensions with the errors lower than 15%.

### 4. Discussion and Interpretation

Martensitic microstructure of the nugget zone is obvious in Fig. 3. To calculate the cooling rate, it is assumed that internal electrode surface temperature is equal to the outlet water temperature.

$T_{max}$  can be calculated through Eq. (1) by setting the temperature of the nugget boundary equals to the liquidus temperature i.e.  $T(z_{FL}) = T_l$ .

Fig. 4 illustrates numerically and analytically computed cooling rates that experienced by three points located at different zones in the welding region: the nugget zone ( $z, r=0$ ), lateral HAZ ( $z=0$  and  $r>r_{FL}$ ) and axial HAZ ( $z>z_{FL}$  and  $r=0$ ). In this figure the variation of cooling rates are plotted versus temperature during the cooling step for the weld created under 10 kA welding current conditions.

Numerical results for points located at the center of the weld zone ( $z, r=0$ ) are given in Fig. 4(a). It is seen that the reliability of analytical model at lower temperatures (about 950°C) increases. The comparison between analytically and numerically predicted cooling rates for a point at axial HAZ ( $z>z_{FL}, r=0$ ) are also depicted in Fig. 4(b). It is seen that, similar to NZ, there are very good agreement between two models especially at temperatures below 850 °C. Temperature history of lateral HAZ can also be estimated by the present analytical model if it is assumed that the temperature profile along the sheet thickness at  $r>r_{FL}$  is similar to  $r=0$ . It is a reasonable assumption but it is mandatory to note that for lateral HAZ ( $r>r_{FL}$ ),  $T_{max}$  in Eqs. (1). and (6) should be replaced by the peak temperature at HAZ. Fig. 4(c) shows the cooling rate variations for a point in lateral HAZ that its peak temperature is 1120 °C. It is seen that at the beginning of cooling, the cooling rate increases rapidly with decreasing of temperature to a maximum value and then with further temperature reduction, cooling rate reduces again. It can be deduced from the above discussion that the analytical model gives reliable results at temperatures below  $T_m/2$ .

Consequently the cooling rate for low temperature transformation ( $T<T_m/2$ ) can be found by differentiating the Eq. (5) with respect to the time as follows:

$$\dot{T} = \frac{\alpha\pi^2}{4h^2}(T - T_s) \quad \text{Eq. (8)}$$

Regarding to this equation, cooling rate of any point at temperatures smaller than  $T_m/2$  is proportional to differences between the studied point temperature and the temperature of the surface sheet.

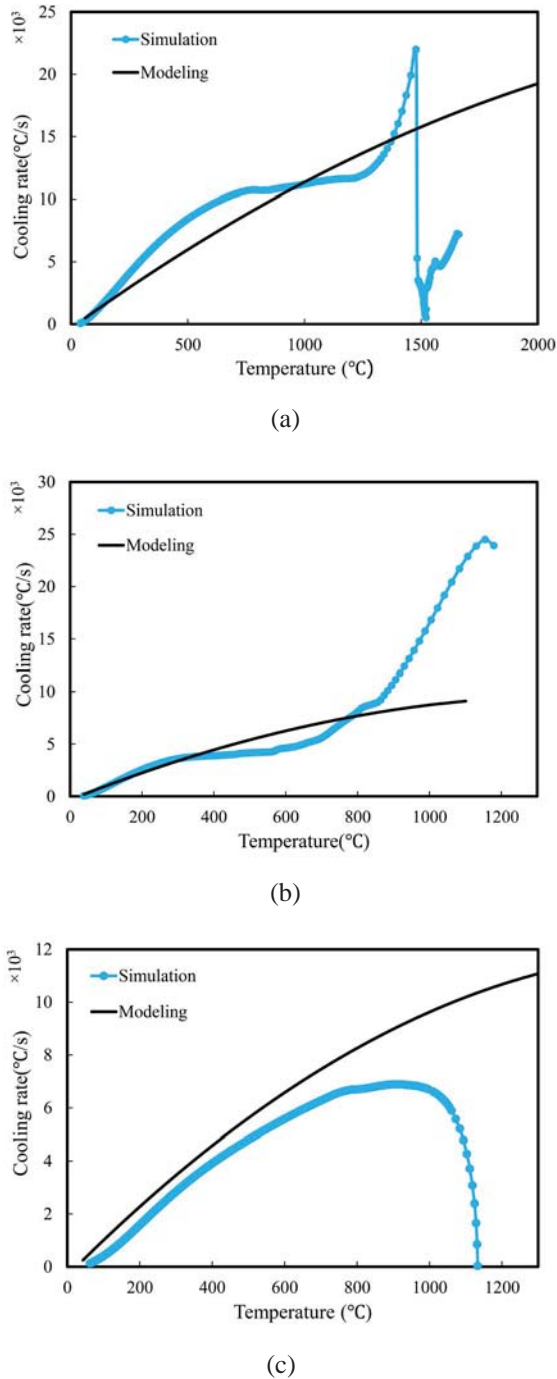


Fig. 4. The cooling rate computed as a function of temperature by analytical and numerical models during the cooling step at different locations of weld zone which created with 10kA. (a)  $z, r=0$ , (b)  $z=0.75 \times h, r=0$  and (c)  $z=0, r > r_{FL}, T_{max}, r=1120 \text{ }^\circ\text{C}$ .

Decomposition of austenite is one of the most important transformations in low alloy steels that should be taken into account as low temperature transformation as compared to solidification temperature range.

“ $\Delta t_{7-4} = t_{700^\circ\text{C}} - t_{400^\circ\text{C}}$ ” parameter is defined as an index for assessment of the average cooling rate during decomposition of austenite temperature range (700 °C - 400 °C) for different points along Z and r axes of the nugget points. Indeed, it is the time that takes any point to pass the critical temperature range. The results for welds created with 10 kA are summarized in Fig. 5. This figure demonstrates that with closing to the nugget center, the cooling rate only slightly increases. This variation can be attributed to the continuous decrease of TS during the austenite transformation. In fact, with closing to the nugget center, decomposition of austenite takes place at the lower  $T_s$  (see Eq. (8)).

This claim is confirmed by observed consistency in the hardness profile along z direction given in Fig. 2. This consistency is reported frequently in other investigations on spot resistance welding of steels [1-2, 16-18]. Consequently the resultant cooling rate from Eq. (8) is reliable for the whole nugget and can be applied for prediction of the nugget microstructure.

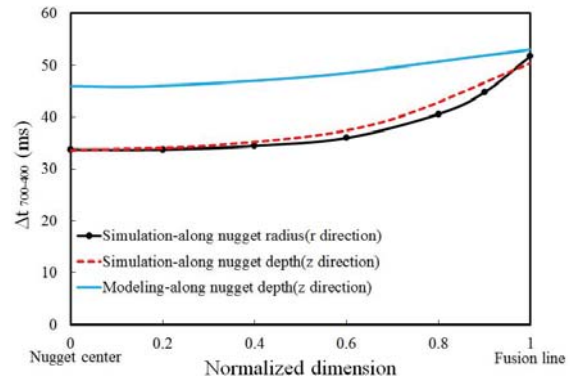


Fig. 5. The numerically and analytically predicted time intervals that different points along r and z axis will

The final microstructure of the nugget can be determined by estimation of cooling rate at the instance of austenite decomposition using Eq. (8) with knowing  $T_s$ . Fig. 6 shows a microstructure map plotted as a function of the sheet thickness and the sheet-electrode interface temperature. The boundary of each region in this map corresponds to the cooling rate limits that resultant microstructure will be changed at these limits when the austenite is cooled from above the upper critical temperature i.e.  $A_3$  (900 °C).

These cooling rates can be derived from CCT diagrams (here it is derived from JMatPro software). Fig. 6 also implies that with increasing the critical cooling rate the extent of martensite region in the map decreases as expected. In this figure the variations of  $T_s$  at the moment of austenite transformation also are illustrated by red arrows for different conditions. Subsequently for all conditions, the cooling rate is high enough to produce a martensitic microstructure in the nugget.

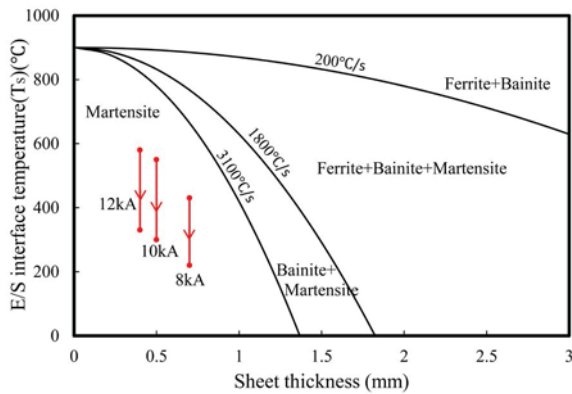


Fig. 6. The microstructure map established versus sheet thickness and electrode-sheet interface temperature (TS) for studied material. The red arrows on this map show the TS variations at the instance of the nugget phase transformation regarding the joint thickness at different welding conditions.

Based upon microstructural analyses and in contrast to our expectations, it is demonstrated that higher welding currents produce a microstructure with higher hardness. This observation can be easily justified by the present analytical model with considering the depth of the electrode indentation (as depicted in Fig. 6). It is well known that higher applied welding currents impose more plastic deformation and in turn deeper electrode indentation. Higher welding current results in higher  $T_{max}$  that it acts as an increasing factor on the cooling rate but it should be mentioned that based on Eq. (8) the cooling rate is inversely proportional to the square of the sheet thickness at welding zone. Accordingly this thickness reduction can give rise to an increase in the cooling rate in spite of higher attained maximum temperature ( $T_{max}$ ) at higher welding currents.

Tensile shear tests reveal that failure occurs at a region outside of the nugget in all samples i.e. failure mode is pull-out failure. Regarding significant thickness reduction at 12 kA (the weld thickness reduce to one sheet thickness), Pull-out failure can be attributed to the higher strength of the nugget zone with martensitic microstructure compared with ferritic base metal. Fig.7-a illustrates the obtained load-displacement curves corresponding to different

welding conditions. It is seen that the load bearing capacity and the failure displacement, i.e. the maximum value of displacement endured by the weld sample before failure during tensile shear test, increases as welding current increases. This observation can be attributed to increasing of the nugget diameter with welding current. The failure stress can be obtained from the load via the following equation<sup>7)</sup>:

$$\sigma_f = 1.27 \frac{P_f}{hd} \quad \text{Eq. (9)}$$

, where  $\sigma_f$  is the fracture stress,  $P_f$  is the failure load and  $d$  is the nugget diameter. The calculations results as depicted in Fig. 7-b show that fracture stress changes slightly with increasing of the welding current from 8 to 12 kA. So according to Fig. 7-b and Eq. (9), it is confirmed that higher failure capacity ( $P_f$ ) at higher welding current mainly attributed to the nugget size ( $h$  and  $d$ ) since  $\sigma_f$  does not change significantly.

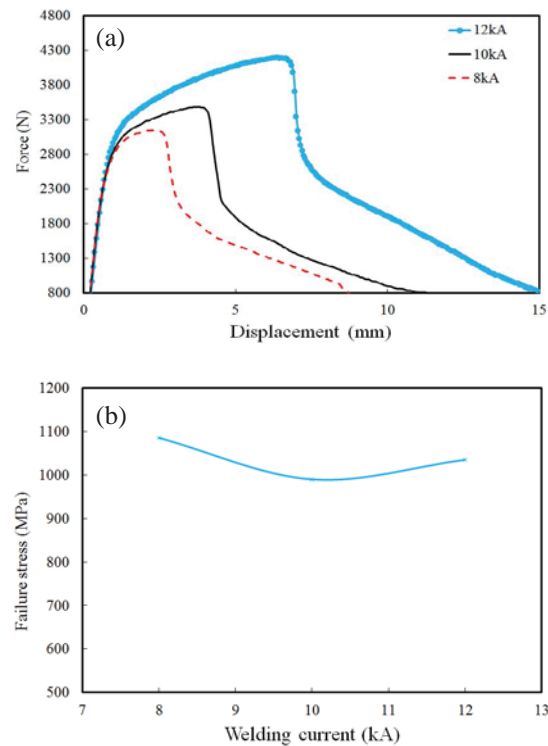


Fig. 7.(a) Load-displacement curves corresponding to different welding conditions and (b) calculated failure stresses as a function of the welding current.

### 5. Conclusions

In summary, an analytical model for prediction of thermal history of RSW is established. It was demonstrated that the analytical model is able to predict the cooling rate of the nugget and HAZ during cooling step especially at temperatures lower

than  $T_m/2$ . The sheet surface temperature at electrode-sheet interface and sheet thickness are recognized as the most important factors influencing the cooling rate. Also a simple approach is proposed for prediction of the weld microstructure based on the analytical model.

## References

- [1]H. Zhang and J. Senkara: Resistance Welding: Fundamentals and Applications, Taylor & Francis CRC Press London, 2005, 141.
- [2]M. Pouranvari and S. P. H. Marashi: Sci. Technol. Weld. Joi., 18(2013), 361.
- [3]Z. Han, J. E. Indacochea, C. H. Chen and S. Bhat: Weld. J., 72(1993), 209-s.
- [4]J. E. Gould: Weld. J., 66(1987), 1s.
- [5]A. Joaquin, A. N. A. Elliott and C. Jiang: Weld. J., 86(2007) 24.
- [6]H. Eisazadeh, M. Hamed and A. Halvae: Mater. Design., 31(2010), 149.
- [7]I.R. Nodeh, S. Serajzadeh and A.H. Kokabi: J. Mater. Process. Technol., 205(2008), 60.
- [8]J. Shen, Y.S. Zhang and X.M. Lai: Sci. Technol. Weld. Joi., 15(2010) 386.
- [9]H. Moshayedi, I. Sattari-Far: J. Mater. Process. Technol., 212(2012), 347.
- [10]N. T. Williams and J. D. Parker: Int. Mater. Rev., 49(2004), 45.
- [11]D. Richard, M. Fafard, R. Lacroix, P. Clery and Y. Maltais: J. Mater. Process. Technol., 132(2003), 119.
- [12]E. Feulvarch, V. Robin and J.M. Bergheau: J. Mater. Process. Technol., 153(2004), 436.
- [13]M. Eshraghi, M.A. Tschopp, M.A. Zaeem and S.D. Felicelli: Mater. Design., 56(2014), 387.
- [14]J. E. Gould, S. P. Khurana and T. Li: Weld. J., 85(2006), 111-s.
- [15]H. Zhigang, W. Yuanxun, L. Chunzhi and C. Chuanyao: Acta Mech. Soli. Sin., 19(2006), 86.
- [16]W. L. Chuko and J. E. Gould, Weld. J., 81(2002), 1s.
- [17]M. I. Khan, M. L. Kuntz, E. Biro and Y. Zhou: Mater. Trans., 49(2008), 1629.
- [18]Y.S. Jong, Y.K. Lee, D.C. Kim, M.J. Kang, I.S. Hwang and W.B. Lee: Mater. Trans., 52(2011), 1330.